# Interfacial properties of high-*k* dielectric $CaZrO_x$ films deposited by pulsed laser deposition

X. Y. Qiu
*Nanjing National Laboratory of Microstructures, Nanjing University, Nanjing 210093, China and Institute of Physics, Southwest University, Chongqing 400715, China*

H. W. Liu, F. Fang, M. J. Ha, Z. G. Liu, and J.-M. Liu[a)]
*Nanjing National Laboratory of Microstructures, Nanjing University, Nanjing 210093, China and International Center for Materials Physics, Chinese Academy of Sciences, Shenyang 110016, China*

(Received 30 November 2005; accepted 18 March 2006; published online 5 May 2006)

The interfacial properties of high-*k* dielectric $CaZrO_x$ thin films deposited by pulsed laser deposition in $O_2$ and $N_2$ ambient are investigated. The $SiO_x$ ($x<2$) interfacial layer is observed for the films deposited at 300 °C in 20 Pa $O_2$. Rapid thermal annealing (RTA) of the films at 700 °C in $N_2$ for 10 s allows for oxidization of the interfacial layers into $SiO_2$ and decomposition of the films into nano-$ZrO_2$ crystals embedded in the matrix of amorphous CaO-rich zirconate. However, by the same RTA, the films deposited at 300 °C in 20 Pa $N_2$ remain amorphous with clean $Si/CaZrO_x$ interface and exhibit good electrical performances. © *2006 American Institute of Physics*.
[DOI: 10.1063/1.2200750]

As the continuous scale down of complementary metal-oxide-semiconductor field effect transistor (CMOS-FET), traditional gate dielectrics cannot meet the requirement of high speed and low power due to large direct tunneling leakage. This problem can be solved by replacing traditional gate dielectrics with higher-*k* dielectrics, such as transition-metal oxides, and their aluminates/silicates.[1] Among the qualifications for high-*k* amorphous dielectrics, two essential issues are the high chemical stability and high anticrystallization temperature $T_s$. $ZrO_2$ has received attentions due to its high chemical stability in contact with Si, high permittivity (20–25), relatively wide band gap (~5.8 eV), and good electrical performances, but its $T_s$ is low ($T_s<500$ °C).[2] Moreover, earlier experiments[3–6] revealed that the chemical reaction between $ZrO_2$ and Si substrate during postannealing usually generates the silicate oxide, metallic Zr clusters, or Zr-silicate (silicide) interfacial layer (IL).

As one of the high-*k* dielectrics candidates, $CaZrO_x$ prepared by pulsed laser deposition (PLD) shows high $T_s$ ($\geqslant$700 °C), high permittivity (~10.5 at 1 MHz), and good electrical performances.[7] In this letter, we investigate the interfacial properties and chemical stability of amorphous $CaZrO_x$ films which are deposited at 300 °C in $O_2$ or $N_2$ ambient of 20 Pa and then submitted into a rapid thermal annealing (RTA) at 700 °C for 10 s in $N_2$ ambient. This RTA scheme is an acceptable postannealing procedure for CMOS-FET,[8] and will be thoroughly employed in our experiments. Additionally, we investigate the electrical properties of the as-prepared $CaZrO_3$ thin films. The $CaZrO_3$ ceramic target for PLD experiment was obtained by conventional sintering method. After ultrasonically cleaned in acetone and de-ionized water, the *n*-type Si(100) substrates with a resistivity of 1–4 Ω cm were etched in a hydrofluoric solution (1:25 $HF:H_2O$) for 2 min to remove native $SiO_2$ layer and leave a H-terminated Si surface. $CaZrO_x$ films were deposited using a KrF excimer laser (Compex 201, 248 nm and 30 ns in wavelength and pulsed width) running at a repeat of 5 Hz with an energy density of ~1.0 $J/cm^2$. The details of the sample preparation were reported earlier.[7] By a huge number of experiments, we optimized the deposition conditions and will focus on two types of samples here. One was deposited at 300 °C in the $O_2$ ambient of 20 Pa (CZO-O films), and the other was deposited at 300 °C in the $N_2$ ambient of 20 Pa (CZO-N films).

For electrical measurements, Pt top electrodes each with an area of $\sim 3.14\times10^{-4}$ $cm^2$ were deposited on the films to form $Pt/CaZrO_x/Si$ MOS structures. The interfacial characteristics of the as-prepared films were studied by high-resolution transmission electron microscopy (HRTEM) and x-ray photoelectron spectroscopy (XPS). The capacitance-voltage (*C-V*) and leakage density-voltage (*J-V*) characteristics of the $Pt/CaZrO_x/Si$ MOS structures were measured using an Agilent 4294A impedance analyzer.[7]

Figure 1(a) shows the cross-section HRTEM image of an as-deposited CZO-O film, which was taken by aligning the electron beam direction along Si [011]. The film is amorphous, but an ~3 nm thick IL between the film and Si substrate is identified. The contrast of the IL is brighter after the RTA on this film is performed [Fig. 1(b)], indicating a remarkable compositional difference of the IL before and after the RTA, as confirmed below by the XPS data. More interestingly, the film also decomposes into nanosized crystals (e.g., areas by arrows A and B) embedded in the amorphous matrix, as shown in Fig. 1(b). The fast Fourier transformation (FFT) and inverse FFT (IFFT) images of these crystals are shown in Figs. 1(c)–1(f), respectively. Following the standard Fourier transformation studies (FTS), it is demonstrated that the evaluated interplanar spacings of 0.30 nm, 0.18 nm, and 0.26 nm correspond to the (111), $(2\bar{2}0)$, and (200) planes of cubic $ZrO_2$, respectively, as shown in Figs. 1(d) and 1(f). This indicates that the nanosized crystals are cubic $ZrO_2$. As a consequence, it is reasonably argued that the amorphous matrix is CaO-rich zirconate, referring to the conservation of mass. Unfortunately, since these crystals are too small to be stable against the long-time radiation of high-

[a)]Author to whom correspondence should be addressed; electronic mail: liuim@nju.edu.cn

 

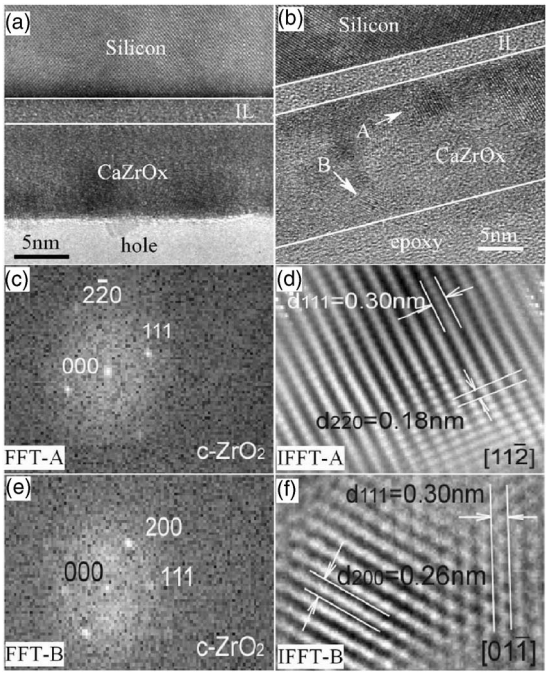


FIG. 1. Cross-section HRTEM images of the CZO-O films (a) before and (b) after the RTA processing. (c)–(f) are the FFT and IFFT images of the selected nanocrystals indicated by arrows A and B in (b), respectively.

energy electron beam during the HRTEM imaging, they quickly become amorphous before we could successfully obtain their dark field images. Moreover, the interfacial layers for the CZO-O samples both before and after the RTA remain amorphous. It is hard to obtain more information from dark field images than from the bright field images. In fact, the bright field images [Figs. 1(a) and 1(b)] already reveal the contrast difference of the ILs before and after the RTA.

On the contrary, even by the RTA treatment, the CZO-N films still remain amorphous and the film/substrate interface is sharp and clean without any IL, as shown in Fig. 2. This indicates that the thermal stability of the CZO-N films is higher than that of the CZO-O films, at least in the present conditions of preparation.

For the XPS analysis, the top layer of each film was etched using Ar ion beam in order to detect the XPS signals from the IL or film/Si interface. All the XPS data were corrected for peak shifts induced by charging effect using the binding energy (BE) of adventitious carbon C1*s* peak (284.6 eV). Figure 3 shows the Si2*p* core-level spectra for the CZO-O films measured before and after the RTA. Besides the Si2*p* level from the Si substrate, we observe two

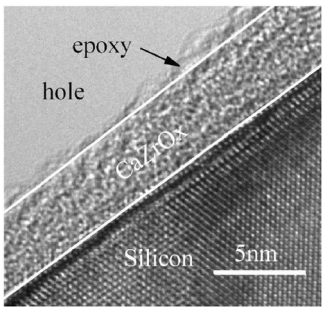


FIG. 2. Cross-section HRTEM images of the CZO-N films after the RTA processing. The film remains amorphous with a clean $CaZrO_x$/Si interface.

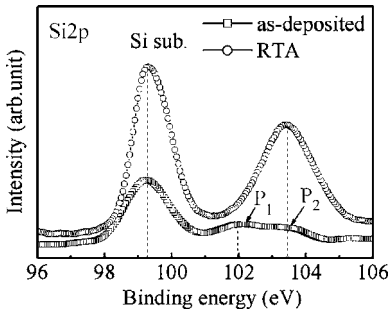


FIG. 3. Si2*p* core-level XPS spectra for the ~3 nm thick CZO-O film before (as deposited) and after the RTA processing.

weak broad peaks ($P_1$ and $P_2$) for the sample before the RTA. $P_1$ peak (~101.9 eV) and $P_2$ peak (~103.4 eV) belong, respectively, to the Si2*p* levels of $SiO_x$ ($x<2$) and $SiO_2$.[9] However, after the RTA treatment, $P_1$ peak disappears and $P_2$ peak becomes much stronger. This implies that the RTA processing allows a full oxidation of the $SiO_x$ IL ($x<2$) into the $SiO_2$ IL.

The fact that a $SiO_x$ IL instead of usual $SiO_2$ is observed for the CZO-O films can be explained as follows. It was reported[10] that oxygen-deficient $ZrO_x$ layer will absorb oxygen from the neighboring $SiO_2$ layer to form fully oxidized $ZrO_2$ layer. A similar kinetic reaction might happen for the present case where the CZO-O films deposited by PLD even in the $O_2$ ambient are also oxygen deficient. The $SiO_2$ IL formed before the deposition will lose some oxygen ions during the subsequent deposition, leading to a subdioxide IL ($SiO_x$, $x<2$). However, the RTA processing makes the CZO-O films partially crystallize. The as-produced grain boundaries enable an accelerated diffusion of residual oxygen into the IL,[11] thus fully oxidizing the $SiO_x$ into the $SiO_2$.

As a comparison, for the CZO-N films, the XPS spectra obtained for the samples before and after the RTA are shown in Fig. 4. A slight rightward shift of the Zr3*d* doublet peaks is detected upon the RTA [Fig. 4(a)]. Apart from the strong Si2*p* peak (from Si substrate), the RTA processing makes the weak Si2*p* peak from the film much stronger and shift a higher BE location (102.6 eV), as shown in Fig. 4(b). This peak belongs to the Si2*p* level of Zr silicate.[12] It implies that during the RTA, Si atoms diffuse from the substrate into the film and react with the nano-$ZrO_x$ precipitates to form Zr-silicate clusters. The kinetics of this reaction is enhanced because for the CZO-N films, no interfacial layer exists and the chemical stability of $ZrO_x$ ($x<2$) in contact with Si is lower than that of $ZrO_2$. Additionally, the as-prepared films are ultrathin (2–3 nm), but the penetration depth of Zr into Si substrate can be up to 25 nm during the RTA processing.[13]

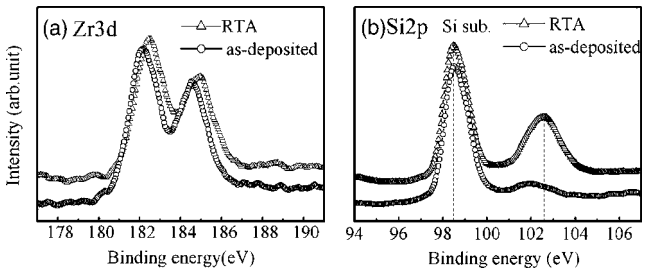


FIG. 4. XPS spectra of (a) Zr3*d* and (b) Si2*p* core levels for the ~3 nm thick CZO-N film before (as deposited) and after the RTA processing.

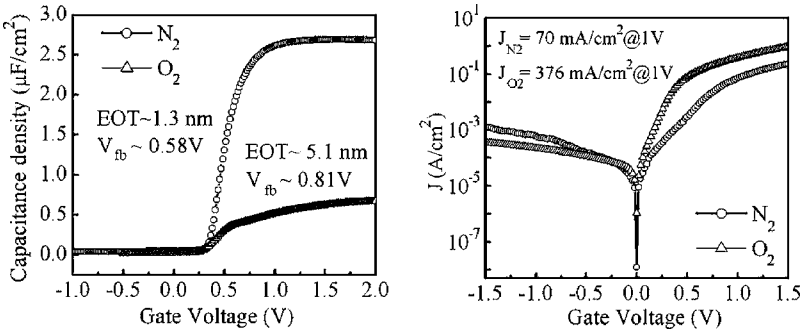


FIG. 5. (a) Capacitance density ($C_{acc}/A$) and (b) leakage current density ($J$) as a function of voltage ($V$) for $Pt/CaZrO_x/n$-Si capacitors with the CZO-N and CZO-O films, respectively. Both the films are ~3 nm thick and undertaken the RTA processing.

The injection of Si atoms into the films at high temperature is also considerable. Thus, this reaction may proceed across the whole ultrathin $CaZrO_x$ layer. After the RTA, the CZO-N films decompose into the mixture of CaO-rich zirconate and Zr-silicate clusters. Because both Zr silicate and $CaZrO_x$ (Ref. 7) have higher $T_s > 700$ °C, the CZO films even after the RTA still remain amorphous (see Fig. 2). The HRTEM and XPS evidences as shown above demonstrate that the CZO-N films have higher $T_s$ and better interfacial property than the CZO-O films.

Subsequently, we compare the electrical properties of the CZO-N and CZO-O films. Figure 5 shows the measured *C-V* and *J-V* curves for two $Pt/CaZrO_x/n$-Si capacitors with a CZO-N film and a CZO-O film, respectively. Both the films are ~3 nm thick and treated by the same RTA (at 700 °C in $N_2$ for 10 s). The actual frequency independent capacitance is calculated from the *C-V* data measured at two high frequencies ($f_1 = 500$ kHz and $f_2 = 1$ MHz) using the method proposed earlier[14] without accounting for quantum mechanical effects. Clearly, the electrical performances of the CZO-N films are much better than those of the CZO-O films, such as small equivalent oxide thickness (EOT) of 1.3 nm, small flatband voltage ($V_{fb}$) of 0.58 V, and low leakage current density ($J$) of 70 mA/cm$^2$ at 1 V gate voltage. The absence of IL and the homogenous amorphous morphology of the CZO-N films contribute to these good electrical properties, while the poor electrical properties of the CZO-O films are attributed to the existence of the IL and phase separation after the RTA treatment, as mentioned above. On the other hand, according to the relation $k = (t/\mathrm{EOT})k_{SiO_2}$, where $t$ is the physical thickness of the $CaZrO_x$ film, the evaluated dielectric constant is $k = 9$ for the CZO-N films after the RTA, slightly smaller than the value $k = 10.5$ for the films before the RTA.[7] The reason may be due to the existence of Zr-silicate clusters in the films after the RTA. In spite of the existence of Zr-silicate clusters, the electrical performances of the CZO-N films are still enough good because Zr silicate is also a good high-$k$ dielectric.

In summary, we have studied the interfacial and electrical properties of $CaZrO_x$ films deposited by pulsed laser deposition at 300 °C in 20 Pa $O_2$ ($N_2$) ambient before and after the RTA at 700 °C in $N_2$ ambient for 10 s. For the films deposited in the $O_2$ ambient, a thin suboxidized $SiO_x$ ($x < 2$) IL is observed between the Si substrate and amorphous films. The RTA processing results in full oxidation of $SiO_x$ into $SiO_2$ and precipitation of nanosized $ZrO_2$ crystals embedded in the matrix of amorphous CaO-rich zirconate. Nevertheless, even by the RTA treatment, the $CaZrO_x$ films deposited in the $N_2$ ambient remain amorphous with clean $Si/CaZrO_x$ interface and exhibit good electrical properties, such as small EOT = 1.3 nm, narrow flatband voltage $V_{fb} = 0.58$ V, and low leakage current density $J = 70$ mA/cm$^2$ at 1 V gate voltage.

This work was supported by the National Natural Science Foundation of China (50528203, 10021001, 60576023, and 10474039) and National Key Projects for Basic Research of China (2004CB619004).

[1] G. D. Wilk, R. M. Wallace, and J. M. Anthony, J. Appl. Phys. **89**, 5243 (2001).
[2] J. Zhu and Z. G. Liu, Appl. Phys. A: Mater. Sci. Process. **78**, 741 (2004).
[3] W.-J. Qi, R. Nieh, E. Dharmarajan, B. H. Lee, Y. Jeon, L. Kang, K. Onishi, and J. C. Lee, Appl. Phys. Lett. **77**, 1704 (2000).
[4] S. K. Dey, C.-G. Wang, D. Tang, M. J. Kim, R. W. Carpenter, C. Werkhoven, and E. Shero, J. Appl. Phys. **93**, 4144 (2003).
[5] T. S. Jeon, J. M. White, and D. L. Kwong, Appl. Phys. Lett. **78**, 368 (2001).
[6] J. Okabayashi, S. Toyoda, H. Kumigashira, M. Oshima, K. Usuda, M. Niwa, and G. L. Liu, Appl. Phys. Lett. **85**, 5959 (2004).
[7] X. Y. Qiu, H. W. Liu, F. Fang, M. J. Ha, X. H. Zhou, and J.-M. Liu, Appl. Phys. A: Mater. Sci. Process. **81**, 1431 (2005).
[8] R. M. C. de Almeida and I. J. R. Baumvol, Surf. Sci. Rep. **49**, 1 (2003).
[9] J. F. Moulder, W. F. Stickle, P. E. Sobol, and K. D. Bomben, *Handbook of X-ray Photoelectron Spectroscopy* (Physical Electronics, Eden Prairie, WI, 1995).
[10] S. J. Wang and C. K. Ong, Appl. Phys. Lett. **80**, 2541 (2002).
[11] S. Ferrari and G. Scarel, J. Appl. Phys. **96**, 144 (2004).
[12] G. B. Rayner, Jr., D. Kang, Y. Zhang, and G. Lucovsky, J. Vac. Sci. Technol. B **20**, 1748 (2002).
[13] M. A. Quevedo-Lopez, M. El-Bouanani, B. E. Gnade, R. M. Wallace, M. R Visokay, M. Douglas, M. J. Bevan, and L. Colombo, J. Appl. Phys. **92**, 3540 (2002).
[14] K. J. Yang and C. M. Hu IEEE Trans. Electron Devices **46**, 1500 (1999).